ACCOUNTS of chemical research

Article

pubs.acs.org/accounts

Two-Dimensional Semiconductor Nanocrystals: Properties, Templated Formation, and Magic-Size Nanocluster Intermediates

Published as part of the Accounts of Chemical Research special issue "2D Nanomaterials beyond Graphene".

Fudong Wang,*[,†] Yuanyuan Wang,[†] Yi-Hsin Liu,[‡] Paul J. Morrison,[†] Richard A. Loomis,[†] and William E. Buhro*[,†]

[†]Department of Chemistry, Washington University, Saint Louis, Missouri 63130-4899, United States

[‡]Department of Chemistry, National Taiwan Normal University, Taipei 11677, Taiwan (ROC)

Supporting Information

CONSPECTUS: Semiconductor nanocrystals having an extended length dimension and capable of efficiently transporting energy and charge would have useful applications in solar-energy conversion and other emerging technologies. Pseudocylindrical semiconductor nanowires and quantum wires are available that could potentially serve in this role. Sadly, however, their defective surfaces contain significant populations of surface trap sites that preclude efficient transport. The very large surface area of long wires is at least part of the problem. As electrons, holes, and excitons migrate along a nanowire or quantum wire, they are exposed to an extensive surface and to potentially large numbers of trap sites.

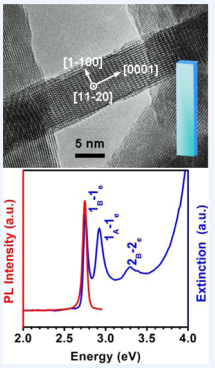

A solution to this dilemma might be found by identifying "long" semiconductor nanocrystals of other morphologies that are better passivated. In this Account, we discuss a newly emerging family of flat semiconductor nanocrystals that have surprising characteristics. These thin, flat nanocrystals have up to micrometer-scale (orthogonal) lateral dimensions and thus very large surface areas. Even so, their typical photoluminescence efficiencies of 30% are astonishingly high and are 2 orders of magnitude higher than those typical of semiconductor quantum wires. The very sharp emission spectra of the pseudo-two-dimensional nanocrystals reflect a remarkable uniformity in their discrete thicknesses. Evidence that excitons are effectively delocalized and hence transported over the full dimensions of these nanocrystals has been obtained. The excellent optical properties of the flat semiconductor nanocrystals confirm that they are exceptionally well passivated.

This Account summarizes the two synthetic methods that have been developed for the preparation of pseudo-two-dimensional semiconductor nanocrystals. A discussion of their structural features accounts for their discrete, uniform thicknesses and details the crystal-lattice expansions and contractions they exhibit. An analysis of their optical properties justifies the sharp photoluminescence spectra and high photoluminescence efficiencies. Finally, a bilayer mesophase template pathway is elucidated for the formation of the nanocrystals, explaining their flat morphologies. Magic-size nanocluster intermediates are found to be potent nanocrystal nucleants, allowing the synthesis temperatures to be decreased to as low as room temperature. The potential of these flat semiconductor nanocrystals in the form of nanoribbons or nanosheets for long-range energy and charge transport appears to be high.

1. INTRODUCTION

Colloidal semiconductor nanocrystals grown from solution are typically isotropically shaped or nearly so. Nanocrystals from the II−VI and IV−VI families exhibit pseudospherical,[1] prolate,[2] or cuboidal[3] morphologies and are often referred to as quantum dots (QDs). Special conditions are required to obtain anisotropic morphologies. Quantum rods (QRs) are produced by rapid growth kinetics[4−6] and selective facet ligation,[7] in which the prolate dimension of QDs is extended. The growth of long nanowires or quantum wires (QWs) requires oriented-attachment[8] or catalyzed[9] mechanisms. Pseudo-zero-dimensional QDs and pseudo-one-dimensional QRs and QWs have been readily available for a wide range of semiconductor materials.

The conditions necessary to produce pseudo-two-dimensional (2D) semiconductor nanocrystals from solution-based chemistry emerged more recently.[10−14] These flat nanocrystals are obtained as nanoribbons (quantum belts or QBs),[11,13,15,16] nanosheets,[14,17] nanoplatelets (quantum platelets or QPs),[10,18−22] and quantum disks.[12,23] Their syntheses are often achieved at quite low temperatures, and *crystalline* CdSe QPs have even been prepared at room temperature.[19] The flat nanocrystals have uniform, discrete thicknesses (1−3 nm) corresponding to integer or half-integer numbers of monolayers of the crystal structure, and lateral dimensions in the range of tens to hundreds of nanometers.

Pseudo-2D semiconductor nanocrystals exhibit remarkable optical properties. Their absorption (extinction) spectra are sharp and assignable to semiconductor quantum-well tran-

Special Issue: 2D Nanomaterials beyond Graphene

Received: August 5, 2014
Published: December 9, 2014

DOI: 10.1021/ar500286j
Acc. Chem. Res. 2015, 48, 13−21

sitions.[10,11,15] The photoluminescence (PL) spectra are also sharp and intense with PL quantum efficiencies (QEs) of 30–80%,[10,13,15,18−20,24−26] which are unusually high for nanocrystals having such large, extended dimensions. Moreover, these nanocrystals are *flat*, with no hints from their crystal structures why they should have grown from solution in these morphologies. Thus, the origins of the flat morphologies, small, discrete thicknesses, and excellent optical properties are of great interest. The syntheses, structures, and formation mechanisms of flat semiconductor nanocrystals are explored herein to reveal the origins of their excellent passivation and optical properties.

2. SYNTHETIC AND STRUCTURAL ASPECTS OF FLAT NANOCRYSTALS

The syntheses of flat colloidal nanocrystals in the II–VI and IV–VI semiconductor families fall into two general categories. One approach employs cadmium-acetate or halide precursors in long-chain amine solvents within a surprisingly low temperature range (25–100 °C).[11,13,17,19,27] Figure 1 shows *crystalline* CdSe QPs synthesized at room temperature.[19]

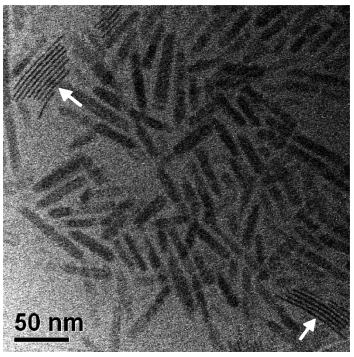

Figure 1. TEM image of pseudo-rectangular, 1.8 nm-thick CdSe QPs prepared in an *n*-octylamine/di-*n*-octylamine cosolvent at room temperature. The white arrows identify bundles of QPs having their broad top and bottom surfaces stacked in parallel, revealing the thin platelet edges. Adapted with permission from ref 19. Copyright 2014 American Chemical Society.

The second approach is conducted with long-chain metal-carboxylate precursors or in the presence of long-chain carboxylic acids within a higher temperature range (≥130 °C for CdSe[10,12,18] and 100 °C for PbS[14]). Interestingly, the flat II–VI nanocrystals obtained from the amine-solvent method exhibit wurtzite (WZ) structures, whereas those prepared by the carboxylate method exhibit zinc blende (ZB) structures.

The precursors and synthetic methods for the pseudo-2D nanocrystals (see Supporting Information) are strikingly similar to those typically employed in standard QD syntheses. A question is how and why these syntheses directed anisotropic growth to afford platelets, ribbons, and sheets, which is addressed in section 4.

Pseudo-2D nanocrystals display several interesting structural features, beyond having morphologies that were unusual for semiconductor nanocrystals until just a few years ago. In some cases, they exhibit lattice contractions or dilations, such that the measured lattice parameters do not match the bulk values (see Supporting Information).

Flat semiconductor nanocrystals are obtained in discrete thicknesses or mixtures of discrete thicknesses, rather than in the continuous size distributions that are typical of QDs and QWs. The discrete character is in part due to the smallness of the thin dimensions, such that the difference, for example, in a 3-ML and 4-ML thickness, is by nature discrete. However, this discrete character also requires extensive intra-nanocrystal thickness uniformity over the large lateral dimensions of the pseudo-2D nanocrystals, the origins of which have not been fully established. A further analysis of this structural issue requires clear definitions of a ML in the ZB and WZ pseudo-2D II–VI nanocrystals.

The flat II–VI nanocrystals having the ZB structure are typically oriented to express (100) facets on the broad top and bottom surfaces.[12,18] Some evidence exists that such nanocrystals may also be oriented with (111) top and bottom facets, but these apparently constitute at most minority populations[12] and are not considered further here. Figure 2a depicts an edge

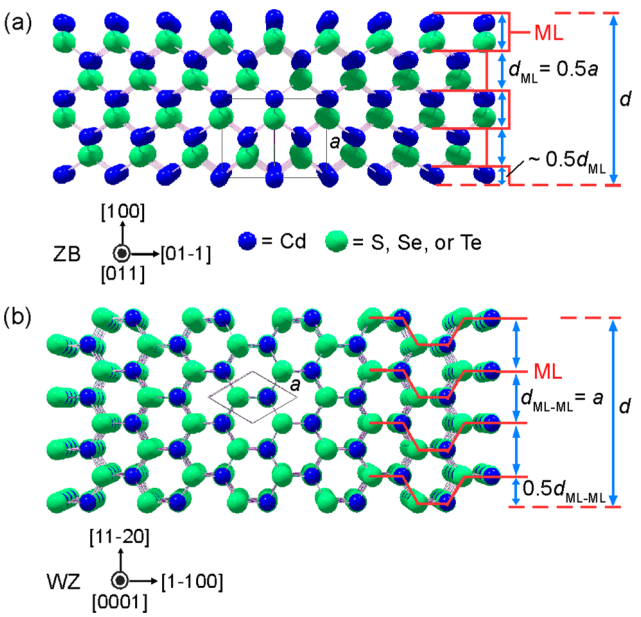

Figure 2. Schematic illustration of the atomic arrangements of the thin edges for pseudo-2D CdE (E = S, Se, or Te) nanocrystals with ZB[12,18] (a) and WZ[11,13] (b) crystal structures. Red solid lines identify the biatomic (Cd–E) monolayers (MLs). d_{ML} (a) and d represent the thickness of a ML and the nanocrystals, respectively. d_{ML-ML} (b) is defined as the inter-ML distance. a is the lattice parameter for the cubic (a) or hexagonal (b) unit cell. Approximately 4.5 and 4 MLs are identified in panels a and b, respectively.

view of a typical ZB pseudo-2D nanocrystal with the thickness dimension oriented vertically. Note that the (100) surfaces are polar; they are constituted entirely of either Cd or Se atoms. The Dubertret and Peng groups agree that both of the top and bottom surfaces are Cd terminated, as depicted in Figure 2a, with a carboxylate ligand bound to each surface Cd atom.[12,18] Peng has pointed out that the Cd termination requires an additional, nonstoichiometric half ML of Cd atoms.[12] Thus, the nanocrystal depicted in Figure 2a has a thickness of 4.5 ML, and by this definition, all such ZB nanocrystals will have half-integer ML thicknesses. Thus, Peng and co-workers reported CdS quantum disks having discrete thicknesses of 4.5, 5.5, 6.5, and 7.5 ML.[23]

Alternatively, the flat II–VI nanocrystals having the WZ structure are oriented to express (11$\bar{2}$0) facets on the broad top and bottom surfaces.[11,13,17,19,27] As is evident in Figure 2b,

DOI: 10.1021/ar500286j
Acc. Chem. Res. 2015, 48, 13–21

these surfaces are *nonpolar*, having equal numbers of Cd and E atoms, and are corrugated. The broad surfaces are populated by Cd−E dimer units. We have chosen to define a ML as the thinnest contiguously bonded network, and so two atomic layers constitute a ML, as shown by the red lines in Figure 2b. As a result, the WZ nanocrystal depicted in Figure 2b consists of 4 MLs, but has a thickness of 3.5 ML because of the corrugated nature of the ML.

Two thickness-related observations, described above, require further understanding. The first is that individual flat nanocrystals possess remarkable intra-nanocrystal thickness uniformity throughout. For example, one could reasonably expect that a flat nanocrystal might have a 3.5-ML thickness in some regions and a 4.5-ML thickness in others of its lateral expanse. We provide further evidence that such intra-nanocrystal thickness variations do not occur in section 3. The second observation is that extensive inter-nanocrystal thickness uniformity is also generally achieved. As noted above, flat nanocrystals are sometimes obtained as mixtures of discrete thicknesses, but conditions may typically be found that produce a single, discrete thickness. The primary synthetic parameter for controlling nanocrystal thickness is the reaction temperature.

Peng and co-workers have presented a nucleation-based, kinetic argument for the exceptional intra-nanocrystal thickness uniformity observed in pseudo-2D nanocrystals.[23] By their argument, the creation of a 2D nucleus on a completed, flat terrace is energetically difficult. That is, there exists a substantial nucleation barrier for initiating growth of a new ML. However, once nucleated, ML growth proceeds rapidly, completing the ML. Thus, the resting state of the flat nanocrystal would consist of entirely flat, completed terraces, hence enforcing intra-nanocrystal thickness uniformity. We suggest that there should also be a thermodynamic component to this thickness uniformity. If a flat nanocrystal were to initially form having regions of varying thicknesses, the resulting kinks and ledges (steps) would be less thermodynamically stable than a completely flat terrace. We should expect such a nanocrystal to ripen to remove the kinks and ledges.

The observation of extensive *inter*-nanocrystal thickness uniformity seems to require that the formation of thicker pseudo-2D nanocrystals becomes progressively more kinetically difficult or thermodynamically costly. The growth of thicker flat nanocrystals generally requires higher growth temperatures. For example, we obtained CdSe QPs having a uniform thickness of 4.5 ML at 25 °C and a uniform thickness of 5.5 ML at 70 °C.[19] Thus, the deposition of the 6th ML on the 4.5-ML thick QPs was either kinetically inhibited or thermodynamically unfavorable at the lower synthesis temperature. In that manner, the thickness is apparently limited to a specific ML value as a function of reaction temperature.

3. OPTICAL PROPERTIES

Among the most exciting, initially surprising discoveries about flat colloidal semiconductor nanocrystals are their very sharp PL spectra and generally high PL QEs.[10,13,15,18−20,24−26] In addition, flat semiconductor nanocrystals exhibit highly structured absorption (extinction) spectra that have been assigned to quantum-well transitions.[10,15,20] We provide an analysis here supporting that assignment. The nature and origins of the unusual optical properties of pseudo-2D nanocrystals are examined in this section. Table S1 (Supporting Information) summarizes the optical properties of these nanocrystals.

3.1. Excitonic vs Quantum-Well Transitions

The absorption (extinction) spectra of flat colloidal nanocrystals are generally sharper and better resolved than those of the corresponding QDs, QRs, or QWs. Because the lateral dimensions of such pseudo-2D nanocrystals are typically large, larger than twice the bulk exciton Bohr radius, quantum confinement exists only in the small, thickness dimension. Thus, quantum platelets, belts, ribbons, or disks having the same thickness exhibit essentially identical absorption spectra.[11−13,17−19] The spectral data for WZ CdSe QPs are discussed here as a representative case.

Figure 3 shows the absorption spectra for WZ CdSe QPs of four discrete thicknesses, corresponding to 4 (1.4 nm), 5 (1.8 nm), 6 (2.2 nm), and 7 (2.6 nm) MLs. Each spectrum contains three well-resolved absorptions, which are assigned in the literature to successive quantum-well transitions.[10,15,20] We confirm that assignment below. Note that as the platelet thickness increases, quantum confinement in that dimension decreases, and the absorptions shift to lower energies accordingly.

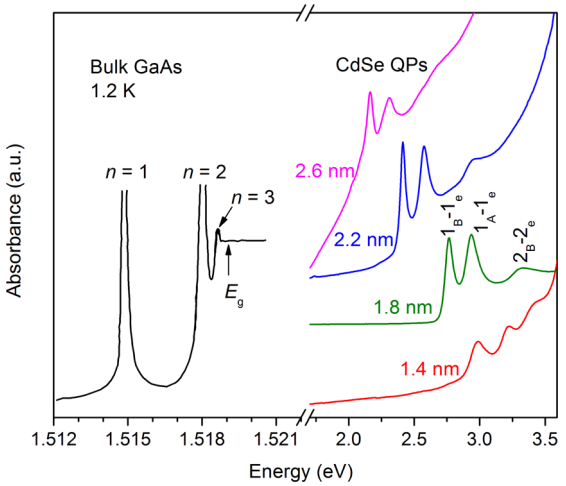

Figure 3. Absorption/extinction spectra of bulk GaAs and WZ CdSe quantum platelets (QPs) having thickness of 1.4, 1.8, 2.2, and 2.6 nm. The GaAs spectrum was adapted with permission from ref 28. Copyright 1991 Wiley-VCH Verlag GmbH & Co. KGaA.

At first glance, the three-feature spectra of the CdSe QPs appear strikingly similar to the low-temperature absorption spectrum of *bulk* GaAs (Figure 3). Of course, bulk GaAs possesses no quantum-confined levels, and the three observed transitions are due to the first three hydrogenic exciton levels associated with the single electron−hole excitation in a bulk semiconductor. Consequently, we should consider whether the structure present in the CdSe QP spectra is also due to hydrogenic exciton levels associated with the first quantum-well transition in the platelets.

If we assume that the three peaks in each QP spectrum (Figure 3) are due to exciton transitions, then the relative energies of the transitions may be determined from eq 1, where E_b is the exciton binding energy, E_g the effective band gap, n the Bohr-model quantum number associated with the exciton transition, and E_n the energy of the transition.[29,30] We may estimate the presumed exciton binding energy from the separation between the lowest-energy transition and the onset of the continuum on the high-energy side of the third peak, which is the putative effective band gap. From the E_g and E_b so

DOI: 10.1021/ar500286j
Acc. Chem. Res. 2015, 48, 13−21

obtained, we may predict the position of the second (n = 2) excitonic transition using eq 1. For the 1.8 nm QPs, the expected position of the second transition so calculated is 3.45 eV, whereas it actually appears at 2.95 eV. Similar discrepancies are obtained for the other QP thicknesses.

$$E_n = E_g - \frac{E_b}{(n - 0.5)^2} \quad (1)$$

Moreover, because of the hydrogenic character of the exciton levels, the transitions should become more closely spaced with increasing n, as is readily apparent in the GaAs spectrum (Figure 3). Simple inspection shows the opposite to be true in the CdSe QP spectra. The asymmetry of the line shapes of the two higher-energy absorption features also suggests these transitions are not associated with transitions to excited hydrogenic exciton levels associated with the lowest quantum-well electron and hole states. The asymmetric shapes of the features resemble Fano line shapes that arise from the Coulombic interaction of a discrete state with a degenerate continuum of excited states. Experimental and theoretical data have illustrated the coupling of such states in quantum wells.[31,32] Discrete hydrogenic exciton transitions to the n = 2 and 3 levels would be expected to have similar, symmetric lineshapes as the lowest-energy n = 1 transition, which we do not observe. Consequently, the transitions may not be assigned to hydrogenic exciton levels and rather appear to follow the pattern expected for particle-in-a-box quantum-confinement states.

Thus, Dubertret and co-workers correctly assigned the two lowest-energy features in the corresponding (and closely similar) ZB CdSe nanoplatelets to the heavy-hole and light-hole transitions associated with the first (n_{Qwell} = 1) quantum-well confinement level, which they labeled hh1-e1, and lh1-e1, respectively.[10] Correspondingly, we assigned the three features in the spectra of WZ CdSe QBs as transitions from the n_{EX} = 1 exciton levels associated with the 1_B-1_e, 1_A-1_e, and 2_B-2_e quantum-well transitions,[15] as shown in Figure 3. (The light-hole and heavy-hole bands in hexagonal semiconductors are typically labeled A and B, respectively.[33]) We may use an effective-mass approximation (eq 2, where h is Planck's constant, d is thickness, and m_e^* and m_h^* are the effective masses of the electron and hole) to estimate the expected energies of these transitions. The $1-1_e$ and 1_A-1_e features for 1.8 nm QBs or QPs are calculated by eq 2 at 2.79 and 2.95 eV, very close to the observed positions (Figure 3). Therefore, the features in the absorption spectra of flat, colloidal nanocrystals are properly assigned to quantum-well transitions, as has been the practice in this field.

$$E_n = E_g + \frac{h^2 n^2}{8d^2}\left[\frac{1}{m_e^*} + \frac{1}{m_h^*}\right] - 4E_b^{bulk} \quad (2)$$

Comparable absorption (extinction) spectra have now been reported for CdS, CdTe, and PbS pseudo-2D nanocrystals.[20−23,27] The light-hole, heavy-hole splitting is small in the spectral data for CdS quantum disks and nanoplatelets,[20,23,27] and nonexistent in the data for PbS QPs.[21]

3.2. Sharp PL Spectra and High PL QEs

The absorption and PL spectra of 1.8 nm-thick WZ CdSe QPs are plotted together in Figure 4 as a representative example. The PL feature is notably sharp, with a fwhm of 50 meV, which is typical of the CdSe QBs and QPs prepared in our laboratory.

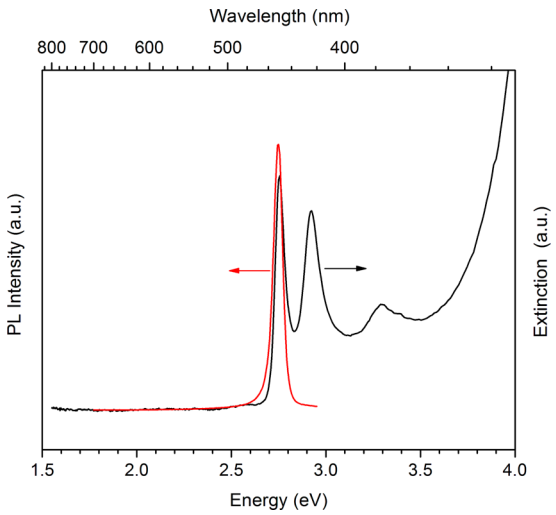

Figure 4. Representative room-temperature PL (red) and extinction (black) spectra of 1.8 nm-thick CdSe QPs.

Dubertret and co-workers have reported a PL fwhm of less than 35 meV for ZB CdSe nanoplatelets (Table S1). For comparison, the larger PL fwhm values for QDs are at the minimum 65−80 meV[34] (typically >90 meV for ensembles of QDs[35,36] and 50−70 meV for single QDs[37]). Those for QRs and QWs are in the range of 75−125 meV.[38,39] The generally sharp PL features observed for flat semiconductor nanocrystals are a testament to their intra- and inter-nanocrystal thickness uniformities, discussed in section 2, and to low densities of trap states that would give rise to an asymmetry in the PL intensity profile toward lower energies.

Additionally, the PL spectra of pseudo-2D nanocrystals exhibit quite small Stokes shifts, often on the order of 0−30 meV (see Table S1, Supporting Information). These are smaller than those characteristic of QD (25−85 meV),[34] QR (40−55 meV),[40] and QW (40−60 meV)[38] specimens, which are often twice as large. For pseudo-2D nanocrystals, an absorption spectrum is an average of the absorption events over the thickness distribution, both inter- and intra-nanocrystal. In contrast, a PL spectrum reveals emission from those spatial domains within the nanocrystals that have the largest thicknesses and thus the lowest energies. The small observed Stokes shifts for flat semiconductor nanocrystals are supporting evidence of the quantized, discrete thicknesses in the specimens; that is, evidence for the *lack* of a thickness distribution.

The PL QEs of pseudo-2D nanocrystals are generally high, routinely on the order of 30%[10,13,15,19,20] and as high as 80% in core−shell nanoplatelets.[26] These values are competitive with those reported for QDs and QRs and orders of magnitude higher than those typical of QWs having an extended length dimension.[41] In our experience, the PL QEs of flat semiconductor nanocrystals are significantly increased by unbundling and ligand exchange/annealing.[15] In the as-synthesized state, the pseudo-2D nanocrystals typically have their broad top and bottom surfaces bundled together in aligned stacks (see section 4).

Because of our prior experience with colloidal semiconductor QWs, which typically exhibit PL QEs of <1%, we were initially stunned to measure QEs in the range of 20−30% in WZ CdSe QBs (nanoribbons).[15] To our thinking, rectangular QBs exhibit higher surface areas than those of pseudocylindrical wires

DOI: 10.1021/ar500286j
Acc. Chem. Res. 2015, 48, 13−21

having equal cross-sectional area, and thus we expected that the PL QEs should be even *lower* in flat nanocrystals than in QWs. Surprisingly, we observed the opposite.

Using fluorescence microscopy, Loomis and co-workers demonstrated that excitons have an equal probability of recombination and emission at all positions along the length of a QB, suggesting that the excitons are freely mobile or delocalized over the full dimensions of the QB.[15] These observations are indicative of excellent surface passivation and the formation of electron−hole pairs that are bound as hydrogenic excitons.

Thus, the PL QE and fluorescence-microscopy results pointed to something interesting about the (low) density or distribution of the exciton or carrier trap sites on WZ CdSe QBs. We searched for them by carefully depositing (growing) Au nanocrystals on the belts.[15] Preferential nucleation of Au on defect sites was expected, and if the trap sites were in proportion to the decorated surface defects, then the trap-site populations could be characterized by such decoration. Indeed, the Au nanoparticles preferentially nucleated on the thin QB *edges*, rather than on the broad top and bottom surfaces (Figure 5).

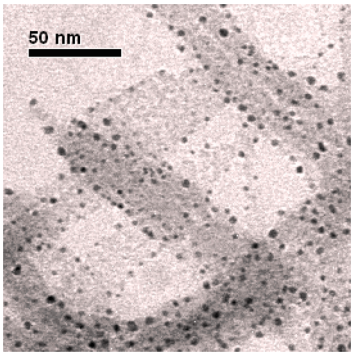

Figure 5. TEM image of CdSe QBs decorated by Au nanoparticles, which are deposited primarily on the edges of the belts. Printed with permission from ref 15. Copyright 2009 American Chemical Society.

Therefore, the decoration experiment suggested that exciton or carrier trap sites were concentrated in the QB edges, which constitute only 14% of the total surface area.[15] The result also indicated that the large top and bottom facets were extremely well passivated. A crystallographic origin for the differential passivation of the edges and top/bottom facets was *not* evident, because *both* types are nonpolar facets containing only slightly different arrangements of Cd−Se dimers. We surmised that the better passivation of the top and bottom facets must result from the growth pathway, which is elucidated in section 4.

4. BILAYER MESOPHASE TEMPLATE PATHWAY

As noted above, the growth of flat colloidal semiconductor nanocrystals from solutions or dispersions is unusual, as such syntheses typically produce QDs or QRs. Flat morphologies are in some cases dictated by crystal structure. For example, compounds having layered crystal structures with van der Waals gaps, such as MoS_2,[42] are often obtained as sheets or platelets. However, the WZ, ZB, and rock-salt (RS) structures of II−VI and IV−VI semiconductors contain no such symmetry-lowering crystallographic features. How then do they grow in highly anisotropic pseudo-2D morphologies?

4.1. In Long-Chain Amine Solvents

Hyeon and co-workers provided considerable insight into this question by characterizing the structure of the spontaneously formed mesophase resulting from the combination of simple cadmium salts such as $CdCl_2$ and long-chain amine solvents such as *n*-octylamine.[17] This combination produces a lamellar amine-bilayer mesophase (Figure 6a) that is readily charac-

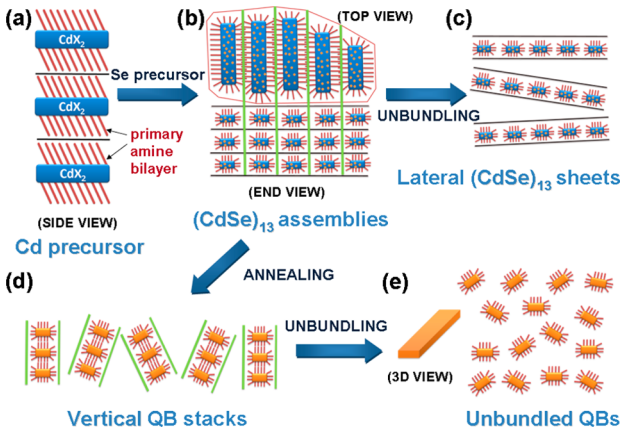

Figure 6. A schematic depiction of the bilayer mesophase template pathway for the formation of colloidal nanosheets, QBs, and QPs. Adapted with permission from ref 13. Copyright 2011, American Chemical Society.

terized by low-angle XRD. The mesophase contains CdX_2 sheets of molecular thickness separated by self-assembled monolayers of amines bound by their NH_2 head groups to the top and bottom surfaces of the sheets. The vertical stacking of such assemblies produces the lamellar amine-bilayer structure.

This anisotropically structured cadmium precursor serves as a template for the nucleation and growth of flat nanocrystals within the planar galleries formed between the amine head groups of the self-assembled monolayers. Hyeon and co-workers reported the formation of CdSe nanosheets[17] and CdS nanoplates[27] from this mesophase template, by reaction of the cadmium species entrained in the planar galleries with elemental Se and S, respectively. We note that the product nanocrystals were initially obtained from the syntheses still assembled into bundles or stacks, reflecting the template structure into which they were organized during growth.

We elucidated a closely related template pathway for the synthesis of CdSe QBs.[13] Dissolution of $Cd(OAc)_2{\cdot}2H_2O$ in *n*-octylamine gave a lamellar amine-bilayer mesophase (Figure 6a), which was clearly evident in low-angle XRD patterns.

Spectroscopic monitoring upon addition of selenourea to Figure 6a precursor at room temperature evidenced the initial formation of a mixture of the magic-size nanoclusters $(CdSe)_{13}$, $(CdSe)_{19}$, $(CdSe)_{33}$, $(CdSe)_{34}$, which equilibrated to $(CdSe)_{13}$ within several hours, paralleling a similar observation by Hyeon and co-workers.[16] Low-angle XRD and TEM images confirmed that the lamellar mesophase remained intact at this intermediate stage (Figure 6b).

Figure 7a is a TEM image of mesophase-assembled $(CdSe)_{13}$ nanoclusters, showing the layered organization on edge as parallel striping. We found that such lamellae were readily peeled apart, and Figure 7b shows single layers removed from the $(CdSe)_{13}$ mesophase assembly (Figure 6c). They exhibited a zebra-stripe pattern of alternating light and dark regions. We surmised that the $(CdSe)_{13}$ nanoclusters were contained within

DOI: 10.1021/ar500286j
Acc. Chem. Res. 2015, 48, 13−21

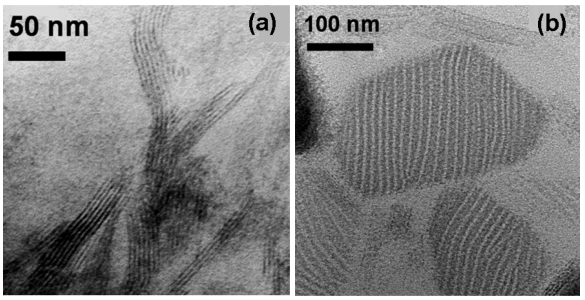

Figure 7. Representative TEM images of bundled (a) and unbundled (b) $(CdSe)_{13}$ nanocluster assemblies. Adapted with permission from ref 13. Copyright 2011 American Chemical Society.

the dark stripes and that the light stripes were amine bilayers. Thus, somewhere between Figure 6a and 6b the template acquired a double-lamellar architecture, with layering in two orthogonal directions (Figure 6b). We later learned that a single-layer thickness of $(CdSe)_{13}$ nanoclusters were assembled into each rectangular gallery of the double-lamellar intermediate.[43]

Upon heating a dispersion of the $(CdSe)_{13}$-intermediate mesophase within the fairly mild temperature range of 85−98 °C, the $(CdSe)_{13}$ nanoclusters coalesced and recrystallized to WZ CdSe QBs.[13] The QBs were obtained in vertically stacked bundles (Figure 6d), indicating that the template in this case disassembled in the orthogonal dimension (to the intermediate mesophase in Figure 6b,c). Subsequent ligand exchange with the longer-chain oleylamine caused the stacked QBs to unbundle into separated nanocrystals (Figure 6e). We established similar growth pathways for CdSe[19] and PbS[21] QPs.

The bilayer mesophase template pathway for nanosheet, QB, and QP growth described here accounts for both the morphologies and the excellent optical properties of pseudo-2D nanocrystals. The nanocrystals are flat because they were templated within planar reaction galleries. The mean widths and thicknesses of the CdSe QBs were very close to the dimensions of the dark stripes within the double-lamellar intermediate mesophase (Figures 6b and 7b) measured from TEM images, establishing that the QB morphology and dimensions were imposed by the template.

Additionally, the bilayer mesophase cadmium precursor (Figure 6a) was constructed of *n*-octylamine self-assembled monolayers. Apparently, the self-assembled monolayer passivation was retained in the $(CdSe)_{13}$-intermediate mesophase (Figure 6b) and ultimately inherited by the broad top and bottom surfaces of the QBs (Figure 6d,e). The kinetic and thermodynamic predisposition of the pseudo-2D nanocrystals toward crystallographically flat top and bottom terraces was discussed in section 2. The two best conditions for achieving electronically well passivated nanocrystals are flat, defect free surfaces and self-assembled-monolayer ligation, both of which resulted adventitiously from the mesophase-template growth pathway. The flat colloidal nanocrystals acquire their excellent optical properties as a consequence of this pathway.

The factors controlling the lateral dimensions within the bilayer mesophase templates are not yet understood. As noted throughout, some of these syntheses produce nanoplatelets or nanosheets, where the lateral dimensions are comparable, and others produce nanoribbons or QBs, having one long and one short lateral dimension. As discussed here, we have shown that nanoribbons and QBs may arise from double-lamellar templates (Figure 6b). Conceivably, nanoplatelets and nanosheets may be templated within single-lamellar mesophases. We have begun experiments intended to alter the dimensions within the templates by varying the compositions of the mesophases, and some results of those efforts are presented in section 5. We recently learned that amine bilayer mesophases may be formed using shorter-chain primary amines,[43] which also template the growth of flat CdSe nanocrystals. An important synthetic advance will be achieved when the thicknesses, widths, and lengths of the pseudo-2D nanocrystals may be purposefully controlled, which will require a better understanding of mesophase template structure.

4.2. Using Long-Chain Metal-Carboxylate Precursors

The reports of the long-chain metal-carboxylate syntheses indicate that the product PbS nanosheets[14] and CdSe nanoplatelets[18] may be obtained initially in bundled stacks analogous to those in Figure 6d. SAXS or low-angle XRD data establish a periodic nanocrystal bilayer stacking, with the bilayer consisting of the long-chain carboxylate ligands bound to the top and bottom facets of the flat nanocrystals. Thus, the observations of these bundled assemblies of product nanocrystals are consistent with their formation within a (carboxylate) bilayer mesophase template.

Furthermore, we re-examined the long-chain carboxylate synthesis of PbS nanosheets reported by Weller and co-workers.[14] We found that combination of three components from the synthesis, $Pb(OAc)_2{\cdot}3H_2O$, oleic acid, and DMF, spontaneously formed a lamellar, oleate-bilayer mesophase at room temperature, analogous to that in Figure 6a.[21] We also monitored the 2D oriented attachment process producing the nanosheets by TEM, finding evidence suggesting that the oriented attachment of initially formed PbS nanoparticles was occurring in a lamellar-template structure.[21] Thus, observations before, during, and after the synthesis were consistent with a bilayer mesophase template pathway.

We note that related template approaches have been discovered in the syntheses of other flat nanocrystals (see Supporting Information). Given the prevalence of lamellar bilayer templating, we strongly suspect that such a mechanism is operative in all syntheses producing flat colloidal semiconductor nanocrystals.

5. MAGIC-SIZE CLUSTERS AND LOW-TEMPERATURE NUCLEATION

As discussed in section 4.1, bilayer mesophase assemblies of magic-size $(CdSe)_{13}$ nanoclusters were intermediates in the templated growth of WZ CdSe QBs. In fact, the intermediate phase depicted in Figure 6b precipitated as a white solid, which we determined to be a pure, ligated form of the nanocluster $[(CdSe)_{13}(n\text{-octylamine})_{13}]$.[13] Its purity was established by a combination of absorption spectroscopy, providing an excellent match to theoretical predictions, mass spectrometry, and elemental analyses (Cd:Se = 1:1). We subsequently prepared a series of $[(CdSe)_{13}(RNH_2)_{13}]$ derivatives, which were the first single-size magic CdSe nanoclusters, identified in the seminal work of Kasuya and co-workers,[44] to be isolated in purified form.[43,45] Given that the nanoclusters contain only weakly bound amine ligands and have the precise CdSe stoichiometry, they are excellent precursors to CdSe nanocrystals in the fairly low temperature range of 85−98 °C.[13]

As a part of our efforts to alter the dimensions within the mesophase templates, we explored Figure 6-like syntheses

DOI: 10.1021/ar500286j
Acc. Chem. Res. 2015, 48, 13−21

conducted in primary amine/secondary amine cosolvent mixtures.[19] To our great surprise, these reactions afforded *crystalline* WZ CdSe QPs (Figure 1) at *room temperature*, hundreds of degrees lower than the conventional synthesis temperatures for CdSe nanocrystals. Spectroscopic monitoring established the key intermediate in the room-temperature synthesis to be the magic-size nanocluster $(CdSe)_{34}$ (Figure 8), which was isolated in purified form as $[(CdSe)_{34}(n\text{-octylamine})_{16}(\text{di-}n\text{-pentylamine})_2]$.

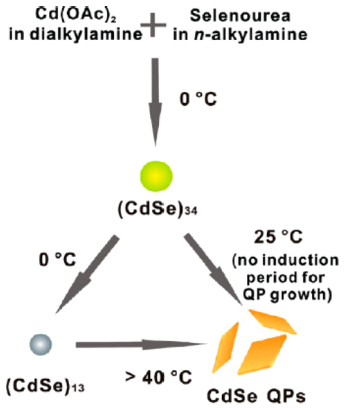

Figure 8. Formation and interconversion of CdSe nanoclusters and QPs in primary amine/secondary amine cosolvent mixtures. Reprinted with permission from ref 19. Copyright 2014 American Chemical Society.

Within the amine-bilayer mesophase template, $(CdSe)_{34}$ is thermodynamically less stable than is $(CdSe)_{13}$ and slowly converted to it below room temperature (Figure 8).[19] However, at 25 °C $(CdSe)_{34}$ converted to crystalline CdSe QPs by first-order kinetics with no induction period. We concluded that $(CdSe)_{34}$ is a more potent nanocrystal precursor than is $(CdSe)_{13}$ because it is close to the critical crystal nucleus size for CdSe and has thus in its formation nearly surmounted the nucleation barrier for CdSe nanocrystal growth. That is, $(CdSe)_{34}$ nanoclusters function as critical-size nuclei (potent nucleating agents) that may be stored in a bottle.

We have not observed magic-size nanocluster intermediates in the template growth of PbS nanosheets,[21] nor to our knowledge have they been observed in the high-temperature long-chain metal-carboxylate precursors. Even so, magic-size nanocluster intermediates are common in nanocrystal syntheses,[13,16,19] and magic-size nanoclusters are now becoming available in a range of semiconductor compositions (see Supporting Information).[16,19,43−45] We should expect them to perform as excellent low-temperature nanocrystal precursors.

6. CONCLUSIONS

We began this Account with several questions about pseudo-2D nanocrystals. How and why are they flat? Why do they have excellent optical properties? Why do they have uniform, discrete thicknesses?

We now know that such nanocrystals are flat because they are templated to be flat during their growth. Their discrete thicknesses of a few to several MLs reflect a kinetic or thermodynamic predisposition to crystallographically flat top and bottom surfaces, upon which steps, kinks, or other structural defects are minimized. This paucity of defects on the large surface-area facets and their self-assembled monolayer passivation are responsible for the high PL QEs, even for pseudo-2D nanocrystals having large lateral dimensions. Finally, the narrow PL features result from the inter- and intra-nanocrystal thickness uniformity resulting from the discrete thicknesses.

We also know that magic-size nanocrystals such as $(CdSe)_{13}$ and $(CdSe)_{34}$ are intermediates in the low-temperature growth of flat semiconductor nanocrystals in certain cases and as such are excellent nanocrystal precursors. Magic-size nanoclusters near to the critical crystal nucleus size for other semiconductor compositions should soon be available and serve as low-temperature nucleants. One can imagine entraining such precursors in other mesophase template geometries to provide low-temperature syntheses of well-passivated nanocrystals having a variety of controlled shapes and compositions.

Because of their excellent passivation and scarcity of surface traps, pseudo-2D semiconductor nanoribbons and nanosheets should be capable of efficiently transporting energy and charge to support a range of emerging applications (see Supporting Information).

■ ASSOCIATED CONTENT

Supporting Information

Synthetic methods for pseudo-2D nanocrystals, lattice contraction and expansion, optical properties, PL lifetime, related template syntheses, and potential applications. This material is available free of charge via the Internet at http://pubs.acs.org.

■ AUTHOR INFORMATION

Corresponding Authors

*E-mail: fwang@wustl.edu.
*E-mail: buhro@wustl.edu.

Notes

The authors declare no competing financial interest.

Biographies

Fudong Wang is a Research Scientist at Washington University in St. Louis. He earned his Ph.D degree in chemistry from Washington University (2007). His research interests include synthesis, characterization, and applications of metallic and semiconductor nanostuctures.

Yuanyuan Wang received his B.S. and M.S in Chemistry from Nanjing University, China. He earned a Ph.D. degree at Washington University in 2014. His research interests include synthesis and characterization of colloidal II−VI magic-size nanoclusters and pseudo-2D nanocrystals.

Yi-Hsin Liu is an Assistant Professor at National Taiwan Normal University. He received his Ph.D. degree in chemistry from Washington University (2010). His research interests include self-assemblies and interfacial growth of semiconductor nanocrystals.

Paul J. Morrison is a Graduate Student at Washington University in St. Louis. He will be earning his Ph.D. in inorganic chemistry in 2014 and is currently studying synthetic routes and mechanisms for IV−VI semiconductor nanocrystals.

Richard A. Loomis is an Associate Professor in the Department of Chemistry at Washington University in Saint Louis. His research focuses on the utilization of frequency- and time-resolved laser spectroscopy to characterize the energetics and dynamics of charge carriers prepared in semiconductor nanostructures.

William E. Buhro is the George E. Pake Professor in Arts & Sciences and the Chair of the Department of Chemistry at Washington

DOI: 10.1021/ar500286j
Acc. Chem. Res. 2015, 48, 13−21

University. His research interests are in semiconductor quantum wires, belts, and platelets and in nanocrystal-growth mechanisms.

■ ACKNOWLEDGMENTS

We are grateful to the National Science Foundation for funding (Grant CHE-1306507 for W.E.B. and Grant DMR-0906966 for R.A.L.). We thank our collaborators and co-workers Prof. Patrick C. Gibbons, Prof. Michael L. Gross, Ms. Ying Zhang, Dr. Virgina L. Wayman, Dr. Henry W. Rohrs, Dr. Daryl E. Giblin, Dr. Jessica Hoy, and Dr. Paul J. Kowalski (Bruker Daltonics), who participated in these studies. We also thank Prof. Li Yang for helpful discussions.

■ REFERENCES

(1) Alivisatos, A. P. Semiconductor Nanocrystals. *MRS Bull.* **1995**, *20*, 23−32.
(2) Murray, C. B.; Norris, D. J.; Bawendi, M. G. Synthesis and Characterization of Nearly Monodisperse CdE (E = Sulfur, Selenium, Tellurium) Semiconductor Nanocrystallites. *J. Am. Chem. Soc.* **1993**, *115*, 8706−8715.
(3) Joo, J.; Na, H. B.; Yu, T.; Yu, J. H.; Kim, Y. W.; Wu, F.; Zhang, J. Z.; Hyeon, T. Generalized and Facile Synthesis of Semiconducting Metal Sulfide Nanocrystals. *J. Am. Chem. Soc.* **2003**, *125*, 11100−11105.
(4) Peng, X. G.; Manna, L.; Yang, W. D.; Wickham, J.; Scher, E.; Kadavanich, A.; Alivisatos, A. P. Shape Control of CdSe Nanocrystals. *Nature* **2000**, *404*, 59−61.
(5) Peng, Z. A.; Peng, X. G. Mechanisms of the Shape Evolution of CdSe Nanocrystals. *J. Am. Chem. Soc.* **2001**, *123*, 1389−1395.
(6) Wang, F.; Buhro, W. E. Morphology Control of Cadmium Selenide Nanocrystals: Insights into the Roles of Di-n-octylphosphine Oxide (DOPO) and Di-n-octylphosphinic Acid (DOPA). *J. Am. Chem. Soc.* **2012**, *134*, 5369−5380.
(7) Manna, L.; Wang, L. W.; Cingolani, R.; Alivisatos, A. P. First-Principles Modeling of Unpassivated and Surfactant-Passivated Bulk Facets of Wurtzite CdSe: A Model System for Studying the Anisotropic Growth of CdSe Nanocrystals. *J. Phys. Chem. B* **2005**, *109*, 6183−6192.
(8) Tang, Z. Y.; Kotov, N. A.; Giersig, M. Spontaneous Organization of Single CdTe Nanoparticles into Luminescent Nanowires. *Science* **2002**, *297*, 237−240.
(9) Wang, F. D.; Dong, A. G.; Sun, J. W.; Tang, R.; Yu, H.; Buhro, W. E. Solution-Liquid-Solid Growth of Semiconductor Nanowires. *Inorg. Chem.* **2006**, *45*, 7511−7521.
(10) Ithurria, S.; Dubertret, B. Quasi 2D Colloidal CdSe Platelets with Thicknesses Controlled at the Atomic Level. *J. Am. Chem. Soc.* **2008**, *130*, 16504−16505.
(11) Joo, J.; Son, J. S.; Kwon, S. G.; Yu, J. H.; Hyeon, T. Low-Temperature Solution-Phase Synthesis of Quantum Well Structured CdSe Nanoribbons. *J. Am. Chem. Soc.* **2006**, *128*, 5632−5633.
(12) Li, Z.; Peng, X. Size/Shape-Controlled Synthesis of Colloidal CdSe Quantum Disks: Ligand and Temperature Effects. *J. Am. Chem. Soc.* **2011**, *133*, 6578−6586.
(13) Liu, Y.-H.; Wang, F.; Wang, Y.; Gibbons, P. C.; Buhro, W. E. Lamellar Assembly of Cadmium Selenide Nanoclusters into Quantum Belts. *J. Am. Chem. Soc.* **2011**, *133*, 17005−17013.
(14) Schliehe, C.; Juarez, B. H.; Pelletier, M.; Jander, S.; Greshnykh, D.; Nagel, M.; Meyer, A.; Foerster, S.; Kornowski, A.; Klinke, C.; Weller, H. Ultrathin PbS Sheets by Two-Dimensional Oriented Attachment. *Science* **2010**, *329*, 550−553.
(15) Liu, Y.-H.; Wayman, V. L.; Gibbons, P. C.; Loomis, R. A.; Buhro, W. E. Origin of High Photoluminescence Efficiencies in CdSe Quantum Belts. *Nano Lett.* **2010**, *10*, 352−357.
(16) Yu, J. H.; Liu, X.; Kweon, K. E.; Joo, J.; Park, J.; Ko, K.-T.; Lee, D. W.; Shen, S.; Tivakornsasithorn, K.; Son, J. S.; Park, J.-H.; Kim, Y.-W.; Hwang, G. S.; Dobrowolska, M.; Furdyna, J. K.; Hyeon, T. Giant Zeeman Splitting in Nucleation-Controlled Doped CdSe:Mn^{2+} Quantum Nanoribbons. *Nat. Mater.* **2010**, *9*, 47−53.
(17) Son, J. S.; Wen, X.-D.; Joo, J.; Chae, J.; Baek, S.-i.; Park, K.; Kim, J. H.; An, K.; Yu, J. H.; Kwon, S. G.; Choi, S.-H.; Wang, Z.; Kim, Y.-W.; Kuk, Y.; Hoffmann, R.; Hyeon, T. Large-Scale Soft Colloidal Template Synthesis of 1.4 nm Thick CdSe Nanosheets. *Angew. Chem., Int. Ed.* **2009**, *48*, 6861−6864.
(18) Ithurria, S.; Bousquet, G.; Dubertret, B. Continuous Transition from 3D to 1D Confinement Observed during the Formation of CdSe Nanoplatelets. *J. Am. Chem. Soc.* **2011**, *133*, 3070−3077.
(19) Wang, Y.; Zhang, Y.; Wang, F.; Giblin, D. E.; Hoy, J.; Rohrs, H. W.; Loomis, R. A.; Buhro, W. E. The Magic-Size Nanocluster $(CdSe)_{34}$ as a Low-Temperature Nucleant for Cadmium Selenide Nanocrystals; Room-Temperature Growth of Crystalline Quantum Platelets. *Chem. Mater.* **2014**, *26*, 2233−2243.
(20) Ithurria, S.; Tessier, M. D.; Mahler, B.; Lobo, R. P. S. M.; Dubertret, B.; Efros, A. L. Colloidal Nanoplatelets with Two-Dimensional Electronic Structure. *Nat. Mater.* **2011**, *10*, 936−941.
(21) Morrison, P. J.; Loomis, R. A.; Buhro, W. E. Synthesis and Growth Mechanism of Lead Sulfide Quantum Platelets in Lamellar Mesophase Templates. *Chem. Mater.* **2014**, *26*, 5012−5019.
(22) Pedetti, S.; Nadal, B.; Lhuillier, E.; Mahler, B.; Bouet, C.; Abecassis, B.; Xu, X.; Dubertret, B. Optimized Synthesis of CdTe Nanoplatelets and Photoresponse of CdTe Nanoplatelets Films. *Chem. Mater.* **2013**, *25*, 2455−2462.
(23) Li, Z.; Qin, H.; Guzun, D.; Benamara, M.; Salamo, G.; Peng, X. Uniform Thickness and Colloidal-Stable CdS Quantum Disks with Tunable Thickness: Synthesis and Properties. *Nano Res.* **2012**, *5*, 337−351.
(24) Ithurria, S.; Talapin, D. V. Colloidal Atomic Layer Deposition (c-ALD) using Self-Limiting Reactions at Nanocrystal Surface Coupled to Phase Transfer between Polar and Nonpolar Media. *J. Am. Chem. Soc.* **2012**, *134*, 18585−18590.
(25) Mahler, B.; Nadal, B.; Bouet, C.; Patriarche, G.; Dubertret, B. Core/Shell Colloidal Semiconductor Nanoplatelets. *J. Am. Chem. Soc.* **2012**, *134*, 18591−18598.
(26) Tessier, M. D.; Mahler, B.; Nadal, B.; Heuclin, H.; Pedetti, S.; Dubertret, B. Spectroscopy of Colloidal Semiconductor Core/Shell Nanoplatelets with High Quantum Yield. *Nano Lett.* **2013**, *13*, 3321−3328.
(27) Son, J. S.; Park, K.; Kwon, S. G.; Yang, J.; Choi, M. K.; Kim, J.; Yu, J. H.; Joo, J.; Hyeon, T. Dimension-Controlled Synthesis of CdS Nanocrystals: From 0D Quantum Dots to 2D Nanoplates. *Small* **2012**, *8*, 2394−2402.
(28) Ulbrich, R. G. Electronic Structure and Properties of Semiconductors. In *Materials Science and Technology*; Schroter, W., Ed.; VCH: Weinheim, Germany, 1991; Vol. *4*, p 65.
(29) Greene, R. L.; Bajaj, K. K.; Phelps, D. E. Energy Levels of Wannier Excitons in GaAs-$Ga_{1-x}Al_xAs$ Quantum-Well Structures. *Phys. Rev. B* **1984**, *29*, 1807−1812.
(30) Bugajski, M.; Reginski, K. Optical Properties of Semiconductor Quantum Wells . *Opto-Electron. Rev.* **1996**, *4*, 83−100.
(31) Glutsch, S.; Chemla, D. S.; Bechstedt, F. Fano Resonances in the Optical Spectra of Semiconductor Quantum Structures. *Phys. Rev. B* **1995**, *51*, 16885−16890.
(32) Oberli, D. Y.; Bohm, G.; Weimann, G.; Brum, J. A. Fano Resonances in the Excitation Spectra of Semiconductor Quantum Wells. *Phys. Rev. B* **1994**, *49*, 5757−5760.
(33) Madelung, O. *Semiconductors-Basic Data*, 2nd revised ed.; Springer: Berlin, 1996.
(34) Qu, L. H.; Peng, X. G. Control of Photoluminescence Properties of CdSe Nanocrystals in Growth. *J. Am. Chem. Soc.* **2002**, *124*, 2049−2055.
(35) Talapin, D. V.; Rogach, A. L.; Kornowski, A.; Haase, M.; Weller, H. Highly Luminescent Monodisperse CdSe and CdSe/ZnS Nanocrystals Synthesized in a Hexadecylamine-Trioctylphosphine Oxide-Trioctylphospine Mixture. *Nano Lett.* **2001**, *1*, 207−211.

DOI: 10.1021/ar500286j
Acc. Chem. Res. 2015, 48, 13−21

(36) Lee, J.; Sundar, V. C.; Heine, J. R.; Bawendi, M. G.; Jensen, K. F. Full Color Emission from II−VI Semiconductor Quantum Dot−Polymer Composites. *Adv. Mater.* **2000**, *12*, 1102−1105.
(37) Gomez, D. E.; van Embden, J.; Mulvaney, P. Spectral Diffusion of Single Semiconductor Nanocrystals: The Influence of the Dielectric Environment. *Appl. Phys. Lett.* **2006**, *88*, No. 154106.
(38) Wang, F. D.; Buhro, W. E. An Easy Shortcut Synthesis of Size-Controlled Bismuth Nanoparticles and Their Use in the SLS Growth of High-Quality Colloidal Cadmium Selenide Quantum Wires. *Small* **2010**, *6*, 573−581.
(39) Li, L.-s.; Hu, J.; Yang, W.; Alivisatos, A. P. Band Gap Variation of Size- and Shape-Controlled Colloidal CdSe Quantum Rods. *Nano Lett.* **2001**, *1*, 349−351.
(40) Manna, L.; Scher, E. C.; Li, L. S.; Alivisatos, A. P. Epitaxial Growth and Photochemical Annealing of Graded CdS/ZnS Shells on Colloidal CdSe Nanorods. *J. Am. Chem. Soc.* **2002**, *124*, 7136−7145.
(41) Glennon, J. J.; Tang, R.; Buhro, W. E.; Loomis, R. A. Synchronous Photoluminescence Intermittency (Blinking) along Whole Semiconductor Quantum Wires. *Nano Lett.* **2007**, *7*, 3290−3295.
(42) Seo, J. W.; Jun, Y. W.; Park, S. W.; Nah, H.; Moon, T.; Park, B.; Kim, J. G.; Kim, Y. J.; Cheon, J. Two-Dimensional Nanosheet Crystals. *Angew. Chem., Int. Ed.* **2007**, *46*, 8828−8831.
(43) Wang, Y.; Liu, Y.-H.; Zhang, Y.; Kowalski, P. J.; Rohrs, H. W.; Buhro, W. E. Preparation of Primary Amine Derivatives of the Magic-Size Nanocluster $(CdSe)_{13}$. *Inorg. Chem.* **2013**, *52*, 2933−2938.
(44) Kasuya, A.; Sivamohan, R.; Barnakov, Y. A.; Dmitruk, I. M.; Nirasawa, T.; Romanyuk, V. R.; Kumar, V.; Mamykin, S. V.; Tohji, K.; Jeyadevan, B.; Shinoda, K.; Kudo, T.; Terasaki, O.; Liu, Z.; Belosludov, R. V.; Sundararajan, V.; Kawazoe, Y. Ultra-Stable Nanoparticles of CdSe Revealed from Mass Spectrometry. *Nat. Mater.* **2004**, *3*, 99−102.
(45) Wang, Y.; Liu, Y.-H.; Zhang, Y.; Wang, F.; Kowalski, P. J.; Rohrs, H. W.; Loomis, R. A.; Gross, M. L.; Buhro, W. E. Isolation of the Magic-Size CdSe Nanoclusters $[(CdSe)_{13}(\text{n-octylamine})_{13}]$ and $[(CdSe)_{13}(\text{oleylamine})_{13}]$. *Angew. Chem., Int. Ed.* **2012**, *51*, 6154−6157.

DOI: 10.1021/ar500286j
Acc. Chem. Res. 2015, 48, 13−21